Geomechanics and Engineering, *Vol. 25, No. 6 (2021) 521-533*
DOI: https://doi.org/10.12989/gae.2021.25.6.521

Upper bound solution of collapse pressure and permanent displacement of 3D tunnel faces using the pseudo-dynamic method and the kinematic approach

Biao Zhang*[1,2], Jin Jiang[3], Dao-bing Zhang[3] and Ze Liu[1]

[1]*School of Civil Engineering, Hunan University of Science and Technology, Hunan 411201, China*
[2]*School of Civil Engineering, Central South University, Hunan 410075, China*
[3]*School of Resource and Environment and Safety Engineering, Hunan University of Science and Technology, Hunan, 411201, China*

(Received October 7, 2020, Revised May 14, 2021, Accepted June 15, 2021)

Abstract. This work presents seismic stability analysis of tunnel faces under three-dimensional (3D) conditions. To consider the temporal and spatial features of seismic force, the pseudo-dynamic approach was employed and incorporated into the 'horn-like' mechanism. According to the limit analysis method and the Hoek-Brown strength criterion, analytical solution of collapse pressure on tunnel faces was derived. The permanent displacement of tunnel face was then calculated by virtue of the Newmark method. The effects of the parameters of seismic force and Hoek-Brown strength criterion on collapse pressure and failure range of tunnel faces were analyzed. The relationship between the Hoek-Brown strength criterion parameters, the supporting force, and the yield acceleration was discussed. Moreover, the permanent displacements at the top, center, and bottom of tunnel faces under seismic effect were examined. This paper proposes a new idea for seismic stability analysis of tunnel faces.

Keywords: Hoek-Brown strength criterion; tunnel faces; supporting force; the Newmark method; the kinematic approach

1. Introduction

Many countries locate at the boundary of plates with frequent crustal movements, and therefore suffering from earthquakes. For instance, the San Andreas Fault in the United States, which has a major earthquake almost every 100 years. The whole country of Japan is in the earthquake zone, such as the Hanshin Earthquake in 1995, the Tokushiro earthquake in 2003 and etc. The Qinghai-Tibet Plateau was hit by the Ya'an earthquake in 2013 and the Wenchuan earthquake in 2008. The damages caused by earthquakes were severe, destroying not only ground buildings but also tunnels and other underground structures. In recent years, because of the severe earthquake consequences on underground structures such as tunnels, engineers have gradually realized the importance of earthquake resistance of underground projects. Therefore, it is of great scientific value and engineering significance to investigate the stability of tunnels under seismic effects.

The upper bound limit analysis method, also known as the kinematic approach, is an effective way to analyze the stability of geotechnical structures. In recent years, it has been introduced into tunnel engineering to analyze its stability (Zhang *et al*. 2018, Fraldi and Guarracino 2012, Khezri *et al*. 2015).

According to the kinematic approach, the logarithmic spiral was introduced to construct the 2D failure mechanism of tunnel faces by Soubra (2002), and the collapse pressure of the tunnel faces was obtained. The calculated results were close to the centrifugal experimental data, which verified the rationality of the 2D failure mechanism. A failure mechanism only composed of logarithmic helical curves, namely 'horn-like' mechanism, was constructed by Subrin and Wong (2002). The collapse pressure of tunnel faces was calculated based on the kinematic approach of limit analysis theory. The approach of 'point to point' was adopted to construct a 3D failure mechanism of tunnel faces by Mollon *et al*. (2010), and the shear strength index at any point of the model was discrete. Considering the kinematic approach, the works were compared with the existing works, and the rationality of the 3D failure mechanism was verified. However, the construction method of this mechanism was complicated and difficult to calculate, which was not easy to be applied in practical engineering. A 3D rotational calculation model of rock tunnel faces was established by Senent *et al*. (2013), in light of the plastic kinematic approach and the Hoek-Brown strength criterion. The supporting reaction force of rock tunnel faces was calculated, and the stability of the rock tunnel faces was shown. For sand tunnel, the kinematic approach was introduced into the construction of the 3D failure mechanism of tunnel faces by Ibrahim *et al*. (2015). The upper bound solution of layered soil collapse pressure was deduced, and the validity of the calculation method was verified by comparing with the numerical simulation results.

Moreover, according to limit analysis method and Hoek-Brown strength criterion, Huang (2019) took the ratio of internal energy dissipation rate to work power of external force as a safety factor. A stability assessment method of tunnel faces for safety factor was proposed. With

*Corresponding author, Ph.D.
E-mail: 1020176@hnust.edu.cn

ISSN: 2005-307X (Print), 2092-6219 (Online)

considering the heterogeneity and anisotropy of soil, a 3D log-spiral failure mechanism of tunnel faces was set up by Zhang and Zhang (2020). The supporting force and failure range of tunnel faces was settled with the kinematic limit analysis approach. To apply the results in practical engineering, an approximate solution for fast calculation of support force was offered. In the study of Zhang *et al*. (2020), a 3D collapse model of soft rock tunnel faces was constructed according to the Hoek-Brown strength criterion and the kinematic approach. The influence of rock mass parameters on the stability of tunnel faces was explored, and the safety grade diagram of supporting design was drawn.

The above results were aimed at the stability of tunnel faces, and a series of valuable results have been obtained. Unfortunately, the above results did not consider the effects of earthquakes. In the design of tunnel, seismic design is indispensable. With the severe damage of earthquake to tunnels in recent years, seismic design of tunnels becomes a hot topic in geotechnical engineering (Abate and Massimino 2017, Pakbaz and Yareevand 2005, Jishnu *et al*. 2016).

By assuming the seismic force as a static force acting on the tunnel faces, Saada *et al*. (2013) constructed the log-spiral curves failure model under the seismic influence. The kinematic approach was introduced to derive the collapse pressure of tunnel faces. By comparing with the results of the failure model, the rationality and superiority of their model were confirmed. According to the quasi-static method, the three-dimensional failure model of tunnel faces under seismic force was constructed by Pan and Dias (2018), and the supporting force of tunnel faces was solved by the kinematic approach. The results show that the influence of seismic force on the supporting force of roadway working face in soft rock is very significant. Zhang (2019) decomposed the seismic force into the horizontal and vertical equivalent static forces, and proposed a 3D random collapse mechanism to consider the randomness of the parameters. The supporting force of the rock tunnel face was computed, which was based on the kinematic approach and the response surface method. It was found that the seismic forces has a great impact on the collapse probability of rock tunnel faces. Based on the quasi-static method, the seismic force was introduced into the tunnel calculation model by Zhang *et al*. (2020). The reliability analysis model of 3D tunnel faces under seismic effects was constructed in light of the kinematic method and the response surface approach. The supporting force and failure probability were calculated, and the influence of seismic force on the reliability of the tunnel faces was determined.

The above literature all employed the quasi-static method to discuss the seismic design of the tunnel faces. There is very few literature on the tunnel face stability by using the pseudo-dynamic method, which is usually used to analyze the seismic stability of slope. Compared with the quasi-static method, the pseudo-dynamic method considers the influence of seismic force in time and space. Based on the pseudo-dynamic method, the effects of expansion angle and horizontal and vertical seismic coefficients on slope stability was analyzed by Eskandarinejad and Shafiee (2011). The pseudo-dynamic method was adopted to introduce horizontal and vertical seismic forces into failure mode of the retaining wall by Wang *et al*. (2011), in which the passive earth pressure of the retaining wall under the seismic dynamic effect was solved. According to pseudo-dynamic method, the influence of horizontal and vertical seismic coefficients on the overturning stability of the retaining wall was studied by Nadukuru and Michalowski (2013). The active earth pressure of the retaining wall under dynamic seismic effect was calculated. Moreover, the critical acceleration of three-dimensional slope failure and the solution method of slope displacement under seismic vibration was calculated.

The pseudo-dynamic method is employed to account for the temporal and spatial characteristics of seismic forces in this paper and the three-dimensional stability analysis of tunnel faces is performed based on the kinematic approach. It can present a new idea for the anti-seismic problem of the tunnel faces.

2. Methodology

At present, when studying seismic stability of geotechnical structures, the quasi-static and pseudo-dynamic methods are widely employed. Compared to the quasi-static method, the pseudo-dynamic method is more robust and accurate since both temporal and spatial effects are considered. While actual seismic waveforms are complex, for brevity, the sinusoidal wave is generally used to simulate the variation law of seismic acceleration in a pseudo-dynamic analysis. The expressions of seismic acceleration in the horizontal and vertical directions respectively are (Chanda *et al*. 2019, Basha and Badu 2010)

$$a_{\mathrm{h}}(z,t) = [1 + (f-1)(H-z) / H]k_{\mathrm{h}}g\sin[\omega(t-(H-z)/v_{\mathrm{s}})] \quad (1)$$

$$a_{\mathrm{v}}(z,t) = [1 + (f-1)(H-z)/H]k_{\mathrm{v}}g\sin\left[\omega\left(t-(H-z)/v_{\mathrm{p}}\right)\right] \quad (2)$$

where, $a_{\mathrm{h}}(z,t)$ and $a_{\mathrm{v}}(z,t)$ refer to the seismic acceleration in the horizontal and vertical directions, respectively. z refers to the buried depth. t refers to the time. v_{s} and v_{p} are propagation velocities of transverse and longitudinal seismic waves.H refers to the depth from the bottom of the tunnel to the surface. f is the amplification coefficient of acceleration amplitude. k_{h} and k_{v} are the seismic acceleration coefficients in the horizontal and vertical directions, respectively. g refers to the acceleration of gravity. ω is the angular velocity, ω=2π/T, and T is the period.

Through studying a large amount of actual engineering data, a strength criterion for rock masses and rocks was proposed by Hoek and Brown, namely the generalized Hoek-Brown strength criterion (Hoek *et al*. 2002).

$$\sigma_1 = \sigma_3 + \sigma_{\mathrm{ci}}\left(m_{\mathrm{b}}\frac{\sigma_3}{\sigma_{\mathrm{ci}}} + s\right)^a \quad (3)$$

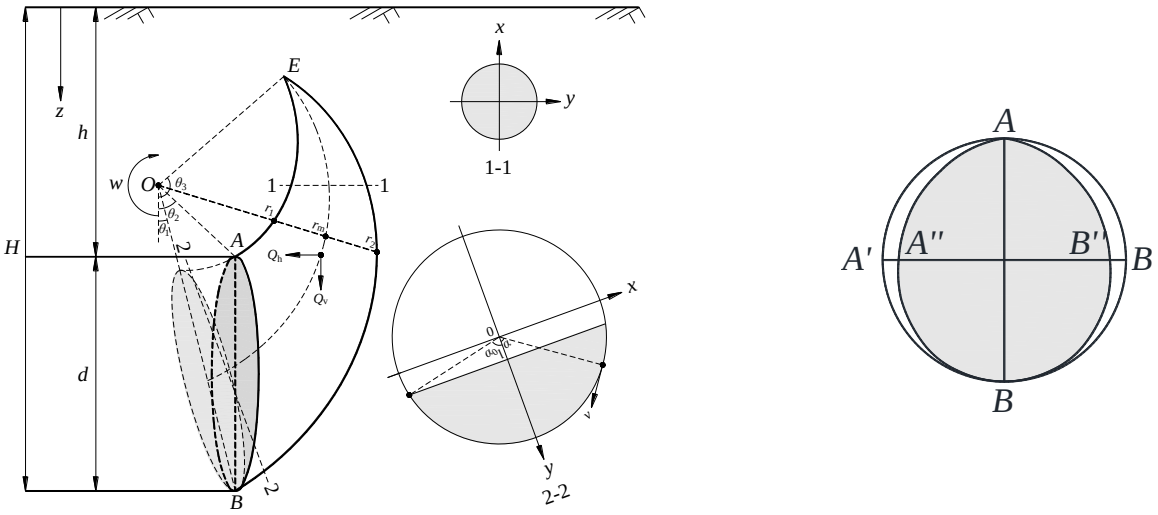

(a) 3D failure mechanism (b) Interface of tunnel face and 'horn'

Fig. 1 3-D failure mechanism of tunnel faces under seismic forces

where, σ_1 and σ_3 are the major and minor effective principle stresses, respectively. σ_{ci} is the uniaxial compressive strength of rock mass. m_b, s and a are dimensionless rock mass parameters, depending on the characteristics of the rock mass. These parameters can be estimated from geological strength index *GSI*, perturbation factor *D*, rock mass constant m_i (Kumar and Rahaman 2020, Huang *et al*. 2019).

$$\begin{cases} m_b = m_i \cdot \exp\left(\dfrac{GSI-100}{28-14D}\right) \\ s = \exp\left(\dfrac{GSI-100}{9-3D}\right) \\ a = \dfrac{1}{2}+\dfrac{1}{6}\left[\exp\left(-\dfrac{GSI}{15}\right)-\exp\left(-\dfrac{20}{3}\right)\right] \end{cases} \tag{4}$$

By introducing the 'tangent method', Zhang *et al*. (2019) derived the equivalent Mohr-Coulomb strength parameters of Hoek-Brown criterion, with the cohesion c_t and friction angle φ_t take the following form.

$$\begin{cases} c_t = \dfrac{m-1}{m} c_0 \left(\dfrac{m\sigma_t \tan\varphi_t}{c_0}\right)^{\frac{1}{1-m}} + \sigma_t \tan\varphi_t \\ \tan\varphi_t = \dfrac{c_0}{m\sigma_t}\left(1+\dfrac{\sigma_n}{\sigma_t}\right) \end{cases} \tag{5}$$

3. Upper bound solution

2.1 3-D failure mechanism of tunnel faces under seismic forces

To introduce the seismic force into the stability analysis mechanism of tunnel faces, the pseudo-dynamic method is adopted. As shown in Fig. 1, it is assumed that the block *AEB* is rotating clockwise around point *O* with angular velocity *w*, under the action of horizontal seismic force Q_h and vertical seismic force Q_v. Tunnel diameter is d and its buried depth is h. In the symmetry plane, *AE* and *BE* are two log-spiral curves with point *O* as the center of rotation, θ_1, θ_2 and θ_3 are the angle of *OB*, *OA*, *OE* with the direction of the vertical line. $r_a=d\sin\theta_1/\sin(\theta_2-\theta_1)$ and $r_b=d\sin\theta_2/\sin(\theta_2-\theta_1)$ refer to the length of *OA* and *OB*. At point *O*, any straight line is made to intersect with the log-spiral curves *AE BE* at two points, and the radial diameters are $r_1(\theta)=r_a\exp[(\theta-\theta_2)\tan\varphi_t]$ and $r_2(\theta)=r_b\exp[(\theta_1-\theta)\tan\varphi_t]$, respectively. Take the two points as the diameter of the vertical central surface to make a circle, r_m is the distance from the center of the circle to point *O*, and the circle formed is the cross-section of the failure mechanism, as shown in Fig. 1-1 and 1-2, in Fig. 1(a). It is worth mentioning that, when constructing the 'horn' failure model of tunnel face in some literature, it is considered that the intersection surface of 'horn' and tunnel face is a circle (Subrin and Wong 2002). In fact, the interface is not round, but pear-shaped, as shown in Fig. 1(b). The expression for area of the interface $S_{AA''BB''}$ will be given later in Eq. (17). The distance from the center of any cross-section of *AEB* (such as the center of section 1-1) to point *O* is shown as

$$r_m = \frac{r_a \exp[(\theta-\theta_2)\tan\varphi_t]}{2} + \frac{r_b \exp[(\theta_1-\theta)\tan\varphi_t]}{2} \tag{6}$$

The diameter of the cross-sectional circle is

$$R = \frac{r_2-r_1}{2} = \frac{r_b \exp[(\theta_1-\theta)\tan\varphi_t]}{2} - \frac{r_a \exp[(\theta-\theta_2)\tan\varphi_t]}{2} \tag{8}$$

Moreover, according to the geometric relationship, the following relation holds:

$$\theta_1+\theta_2-2\theta_3 = \frac{\ln(\sin\theta_1/\sin\theta_2)}{\tan\varphi_t} \tag{9}$$

$$R\cos\alpha_0 = l \tag{10}$$

$$r_m + l = r_a \sin\theta_2/\sin\theta \tag{11}$$

$$v = \omega(r_m+y) = \omega\left\{\frac{r_a \exp[(\theta-\theta_2)\tan\varphi_t]}{2} + \frac{r_b \exp[(\theta_1-\theta)\tan\varphi_t]}{2} + y\right\} \tag{12}$$

$$dV = (r_m+y)dxdyd\theta = \left\{\frac{r_a \exp[(\theta-\theta_2)\tan\varphi_t]}{2} + \frac{r_b \exp[(\theta_1-\theta)\tan\varphi_t]}{2} + y\right\} dxdyd\theta \tag{13}$$

2.2 Assumptions

According to the existing literature, when the kinematic approach was used to study the seismic resistance of geotechnical engineering, the following assumptions should be introduced (Fraldi and Guarracino 2012, Zhang *et al.* 2020): (1) The sliding block *AEB* is a rigid block, and thus internal energy dissipates along the velocity detaching line. (2) The tunnel is deep enough that the sliding block *AEB* is always below the surface. (3) The supporting force of the tunnel faces is evenly distributed. (4) The strength of rock mass is not affected by seismic forces.

2.3 Rates of external work and internal energy dissipation

The work rate generated by the weight of sliding block *AEB*, $\dot{W}_\gamma$, which can be expressed as

$$\begin{aligned}\dot{W}_\gamma &= 2\omega\gamma(f_1+f_2)\\ &= 2\omega\gamma\int_{\theta_2}^{\theta_3}\mathrm{d}\theta\int_{-R}^{R}\mathrm{d}y\int_0^{\sqrt{R^2-y^2}}(r_\mathrm{m}+y)^2\sin\theta\,\mathrm{d}x\\ &\quad+2\omega\gamma\int_{\theta_1}^{\theta_2}\mathrm{d}\theta\int_{l}^{R}\mathrm{d}y\int_0^{\sqrt{R^2-y^2}}(r_\mathrm{m}+y)^2\sin\theta\,\mathrm{d}x\end{aligned} \tag{14}$$

The total work rate $\dot{W}_\mathrm{e}$ is decomposed into the work rate by horizontal seismic force $\dot{W}_{\mathrm{e}1}$ and the vertical seismic force $\dot{W}_{\mathrm{e}2}$, the expression is

$$\begin{aligned}\dot{W}_e &= \dot{W}_{e1}+\dot{W}_{e2}\\ &= \frac{2\omega\gamma}{g}[a_h(f_3+f_4)+a_v(f_1+f_2)]\\ &= \frac{2\omega\gamma}{g}[1+(f-1)(H-z)/H]k_hg\,sin[\omega(t\\ &\quad-(H-z)/v_s)](f_3+f_4)+\\ &\quad\frac{2\omega\gamma}{g}[1+(f-1)(H-z)/H]k_vg\,sin\big[\omega\big(t\\ &\quad-(H-z)/v_p\big)\big](f_5+f_6)\\ &= \frac{2\omega\gamma}{g}[1+(f-1)(H-z)/H]k_hg\,sin[\omega(t\\ &\quad-(H-z)/v_s)]\cdot\\ &\quad\left[\int_{\theta_2}^{\theta_3}d\theta\int_{-R}^{R}dy\int_0^{\sqrt{R^2-y^2}}(r_m+y)^2cos\theta\,dx\right.\\ &\quad+\int_{\theta_1}^{\theta_2}d\theta\int_{l}^{R}dy\int_0^{\sqrt{R^2-y^2}}(r_m\\ &\quad\left.+y)^2cos\theta\,dx\right]+\\ &\frac{2\omega\gamma}{g}[1+(f-1)(H-z)/H]k_vg\,sin\big[\omega\big(t-(H-z)/v_p\big)\big]\cdot\\ &\quad\left[\int_{\theta_2}^{\theta_3}d\theta\int_{-R}^{R}dy\int_0^{\sqrt{R^2-y^2}}(r_m+y)^2sin\theta\,dx+\right.\\ &\quad\left.\int_{\theta_1}^{\theta_2}d\theta\int_{l}^{R}dy\int_0^{\sqrt{R^2-y^2}}(r_m+y)^2sin\theta\,dx\right]\end{aligned} \tag{15}$$

The work rate by supporting force is the product of the supporting force and the velocity, and the expression is shown as

$$\dot{W}_\mathrm{T}=-\sigma_\mathrm{T}\int_{\theta_1}^{\theta_2}\mathrm{d}\theta\int_0^{\sqrt{R^2-l^2}}\frac{2\omega(r_\mathrm{m}+l)^2\cos\theta}{\sin\theta}\mathrm{d}x=-2\sigma_\mathrm{T}\omega f_5 \tag{16}$$

where, the area S_AB formed by the intersection of the failure block *AEB* and the tunnel faces is

$$S_{\mathrm{AA''BB''}}=\int_{\theta_1}^{\theta_2}\mathrm{d}\theta\int_0^{\sqrt{R^2-l^2}}\frac{2(r_\mathrm{m}+l)}{\sin\theta}\mathrm{d}x \tag{17}$$

The internal dissipated work rate $\dot{W}_\mathrm{V}$ only occurs on the velocity discontinuity surface, and the expression is as follows

$$\begin{aligned}\dot{W}_\mathrm{V} &= \int_{\theta_2}^{\theta_3}\mathrm{d}\theta\int_0^{\pi}2\omega c_\mathrm{t}R(r_\mathrm{m}+R\cos\alpha)^2\,\mathrm{d}\alpha\\ &\quad+\int_{\theta_1}^{\theta_2}\mathrm{d}\theta\int_0^{\alpha_0}2\omega c_\mathrm{t}R(r_\mathrm{m}+R\cos\alpha)^2\,\mathrm{d}\alpha\\ &= 2\omega c_\mathrm{t}(f_6+f_7)\end{aligned} \tag{18}$$

where f_1~f_7 take the following form

$$f_1=\int_{\theta_2}^{\theta_3}\mathrm{d}\theta\int_{-R}^{R}\mathrm{d}y\int_0^{\sqrt{R^2-y^2}}(r_\mathrm{m}+y)^2\sin\theta\,\mathrm{d}x \tag{19}$$

$$f_1=\int_{\theta_2}^{\theta_3}\mathrm{d}\theta\int_{-R}^{R}\mathrm{d}y\int_0^{\sqrt{R^2-y^2}}(r_\mathrm{m}+y)^2\sin\theta\,\mathrm{d}x \tag{20}$$

$$f_3=\int_{\theta_2}^{\theta_3}\mathrm{d}\theta\int_{-R}^{R}\mathrm{d}y\int_0^{\sqrt{R^2-y^2}}(r_\mathrm{m}+y)^2\cos\theta\,\mathrm{d}x \tag{21}$$

$$f_4=\int_{\theta_1}^{\theta_2}\mathrm{d}\theta\int_{l}^{R}\mathrm{d}y\int_0^{\sqrt{R^2-y^2}}(r_\mathrm{m}+y)^2\cos\theta\,\mathrm{d}x \tag{22}$$

$$f_5=\int_{\theta_1}^{\theta_2}\mathrm{d}\theta\int_0^{\sqrt{R^2-l^2}}(r_\mathrm{m}+l)^2\cos\theta/\sin\theta\,\mathrm{d}x \tag{23}$$

$$f_6=\int_{\theta_2}^{\theta_3}\mathrm{d}\theta\int_0^{\pi}R(r_\mathrm{m}+R\cos\alpha)^2\,\mathrm{d}\alpha \tag{24}$$

$$f_7=\int_{\theta_1}^{\theta_2}\mathrm{d}\theta\int_0^{\alpha_0}R(r_\mathrm{m}+R\cos\alpha)^2\,\mathrm{d}\alpha \tag{25}$$

2.4 Upper bound solution of collapse pressure and supporting force

According to the principle of virtual power, combined with Eqs. (14)-(16) and Eq. (18), the rates of external force is equal to the dissipation rate of internal energy. The expression of supporting force subjected to seismic force can be obtained.

$$\begin{aligned}\sigma_\mathrm{T} &= \frac{\dot{W}_\mathrm{V}-\dot{W}_\gamma-\dot{W}_\mathrm{e}}{\int_{\theta_1}^{\theta_2}\mathrm{d}\theta\int_0^{\alpha_0}R(r_\mathrm{m}+R\cos\alpha)^2\,\mathrm{d}\alpha}\\ &= \frac{c_\mathrm{t}(f_6+f_7)-\gamma(f_1+f_2)-\frac{\gamma}{g}[\alpha_\mathrm{h}(f_3+f_4)+\alpha_\mathrm{v}(f_1+f_2)]}{f_7}\end{aligned} \tag{26}$$

Moreover, the constraint conditions are

$$\text{subjected to}\begin{cases}0<\theta_1<\theta_2<\pi/2\\ \theta_2<\theta_3<\pi\\ r_\mathrm{a}<r_\mathrm{b}\end{cases} \tag{27}$$

Under the constraint of Eq. (27), the minimum solution of supporting force σ_T in Eq. (26) can be solved by the sequential quadratic programming algorithm in Matlab, and it is also the optimal upper bound solution of supporting force. In the state of ultimate failure, the optimal upper limit

solution of supporting force is equal to the collapse pressure on the tunnel faces, $\sigma_T=\sigma_0$.

4. Verification

Regardless of seismic force, Senent *et al*. (2013) obtained the surrounding rock pressure of the fractured rock tunnel faces. Under the same conditions, rock mass bulk density γ=25 kN/m^3, tunnel diameter d=10m, disturbance parameter D=0, and without seismic force $a_h(z,t)=a_v(z,t)=0$, the kinematic approach is used to solve the surrounding rock pressure of tunnel faces in this paper, as shown in Table 1. Among the 22 groups of data, the surrounding rock pressure of this paper is very close to the results of existing finding (Senet *et al*. 2013), which verifies the feasibility of the 3D 'horn' failure mode. It is worth noting that the comparison results of surrounding rock pressure in Table 1 are relatively similar, with only a small error. The difference does not indicate that the result of the literature (Senet *et al*. 2013) is better and more stable. The reason for this difference is that the method of constructing the 'horn' mode is different. Based on the point-to-point method, the 'horn' model was constructed by Senet *et al*. (2013). However, in this paper, the 'horn' model was constructed by Michalowski's method (Michalowski and Nadukuru 2013, Zhang *et al*. 2020). Therefore, the small error proves that the failure model in this paper is feasible.

Table 1 Comparison of calculation results

Number	*GSI*	m_i	σ_{ci}/MPa	σ_0/kPa		
				Present solutions	Exiting finding (Senet *et al*. 2013)	Error
1	10	5	1	47.6	49.5	-1.9
2	15	5	1	33.1	34.9	-1.6
3	20	5	1	24.7	25.6	-0.9
4	25	5	1	19.1	19.1	0
5	10	5	5	16.6	16.4	0.2
6	15	5	5	10.6	9.4	1.2
7	20	5	5	6.9	5.2	1.7
8	25	5	5	4.4	2.3	2.1
9	10	5	10	10.1	8.4	1.7
10	15	5	10	5.6	3.4	2.2
11	20	5	10	2.7	Stable	-
12	25	5	10	0.5	Stable	-
13	10	5	15	7.0	5.2	1.8
14	15	5	15	3.1	0.1	3.0
15	20	5	15	0.5	Stable	-
16	25	5	15	Stable	Stable	-
17	10	5	20	5	2.3	2.7
18	15	5	20	1.4	Stable	-
19	20	5	20	Stable	Stable	-
20	25	5	20	Stable	Stable	-
21	10	10	1	25.4	26.3	-0.9
22	10	15	1	18.1	18.1	0

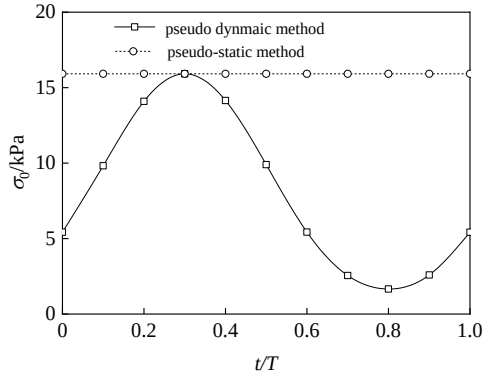

(a) ζ=0

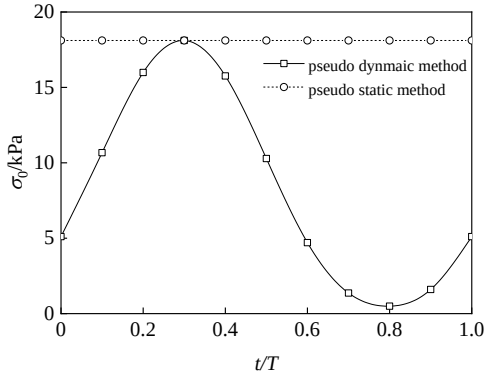

(b) ζ=0.5

Fig. 2 Time domain waveform of surrounding rock pressure

5. Discussion of results

5.1 Collapse pressure and failure range

5.1.1 Time domain waveform

Following parameters are employed: depth ratio of the tunnel H/d=2, rock bulk density γ=25kN/m^3, rock mass constant m_i=15, disturbance parameter D=0, uniaxial compressive strength σ_{ci}=5MPa, geological strength index GSI=20, horizontal acceleration coefficient k_h=0.3, amplification parameter f=1. Both the vertical acceleration proportional coefficient ζ=0 and ζ=0.5 are considered. The time domain waveform of surround rock pressure is obtained based on both the quasi-static and psudo-dynamic methods. The surrounding rock pressure is in a horizontal straight line and does not change with time in Fig. 2, because the amplification effect and time domain of seismic load are not considered. Whereas, in the analysis by the pseudo-dynamic method, the surrounding rock pressure changes in the form of sinusoidal wave, the first half period is 0~0.6T, and the second half period is 0.6T~1.0T. When t=0 and t=1T, the surrounding rock pressure is the same, and the maximum and minimum solutions to surrounding rock pressure are at 0.3T and 0.8T, respectively. The results of the pseudo-dynamic method and the quasi-static method are equal when $t\approx$0.3T. Therefore, the quasi-static method does not consider the amplification effect of seismic force and its locality in the time domain, and it is a particular case of the pseudo-dynamic method. Compared with ζ=0, when ζ=0.5, the amplitude of the time domain waveform of the

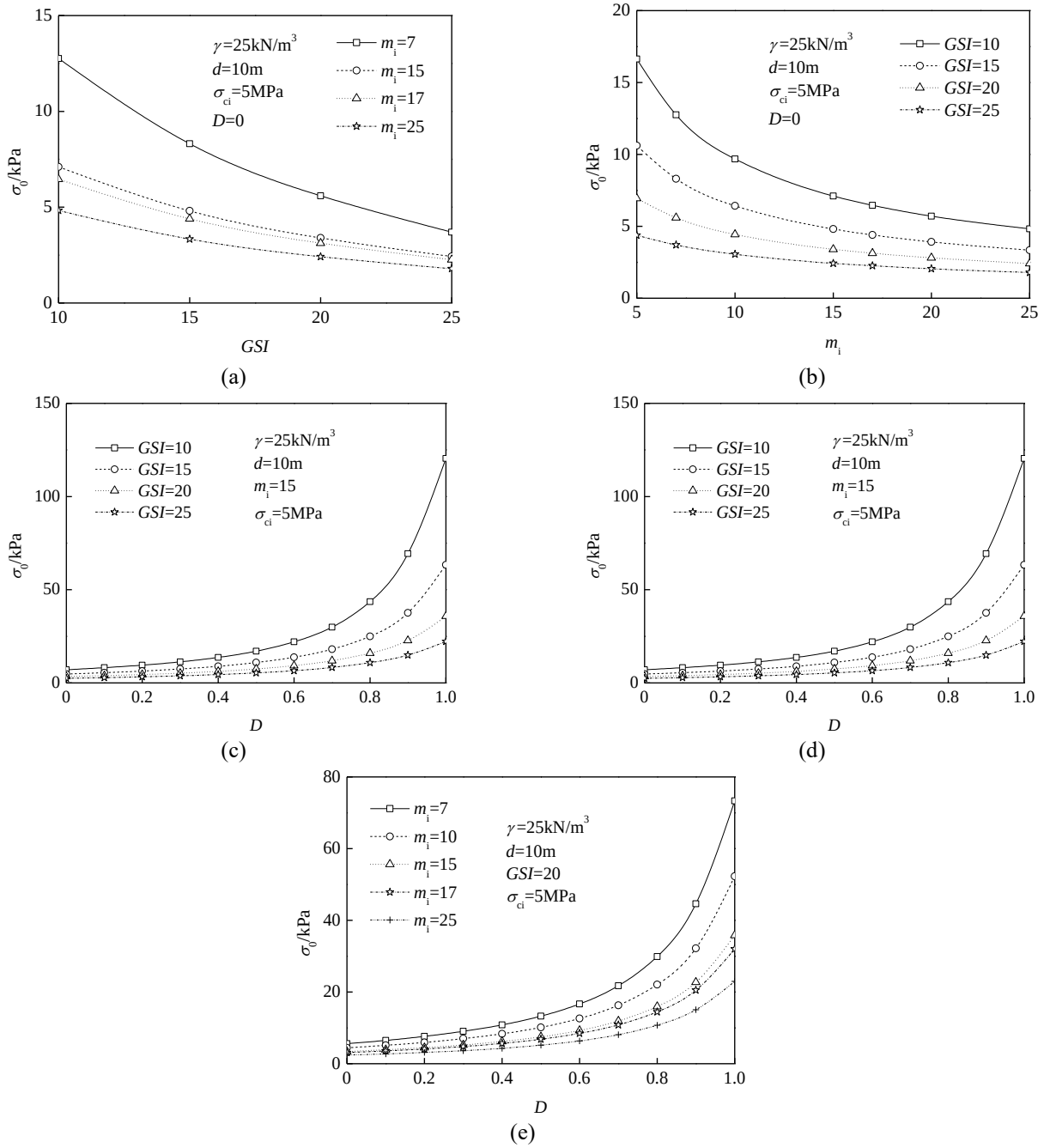

Fig. 3 Influence of Hoek-Brown criterion parameters on surrounding rock pressure

surrounding rock pressure is more immense. Therefore, the ratio coefficient of vertical acceleration ζ has a significant influence on the surrounding rock pressure of tunnel faces.

5.1.2 Condition without seismic effects

When there is no seismic force k_h=0, ζ=0, the effects of the parameters of rock mass on the surrounding rock pressure and failure range of the tunnel faces are shown in Fig. 3 and Fig. 4, respectively.

As shown in Fig. 3, when *GSI*, m_i, and σ_{ci} increase, the surrounding rock pressure σ_0 decreases nonlinearly, and the decreasing trend decreases sharply. Thus, the parameters of soft rock mass have a significant effect on the surrounding rock pressure. The surrounding rock pressure increases nonlinearly when the disturbance factor increases, and the increasing trend becomes steeper, indicating that the disturbance has a significant effect on the surrounding rock pressure.

As can be seen in Fig. 4, when *GSI*, m_i, σ_{ci} decrease or *D* increases, the failure range of tunnel faces increases. This is mainly reflected in that the failure face extends outward along the direction of tunnel excavation, and the failure height, namely the peak of the failure block, also rises.

5.1.3 Condition with only horizontal seismic effect

When there is only horizontal seismic force, the influences of Hoek-Brown criterion parameters on the surrounding rock pressure and failure range of the tunnel

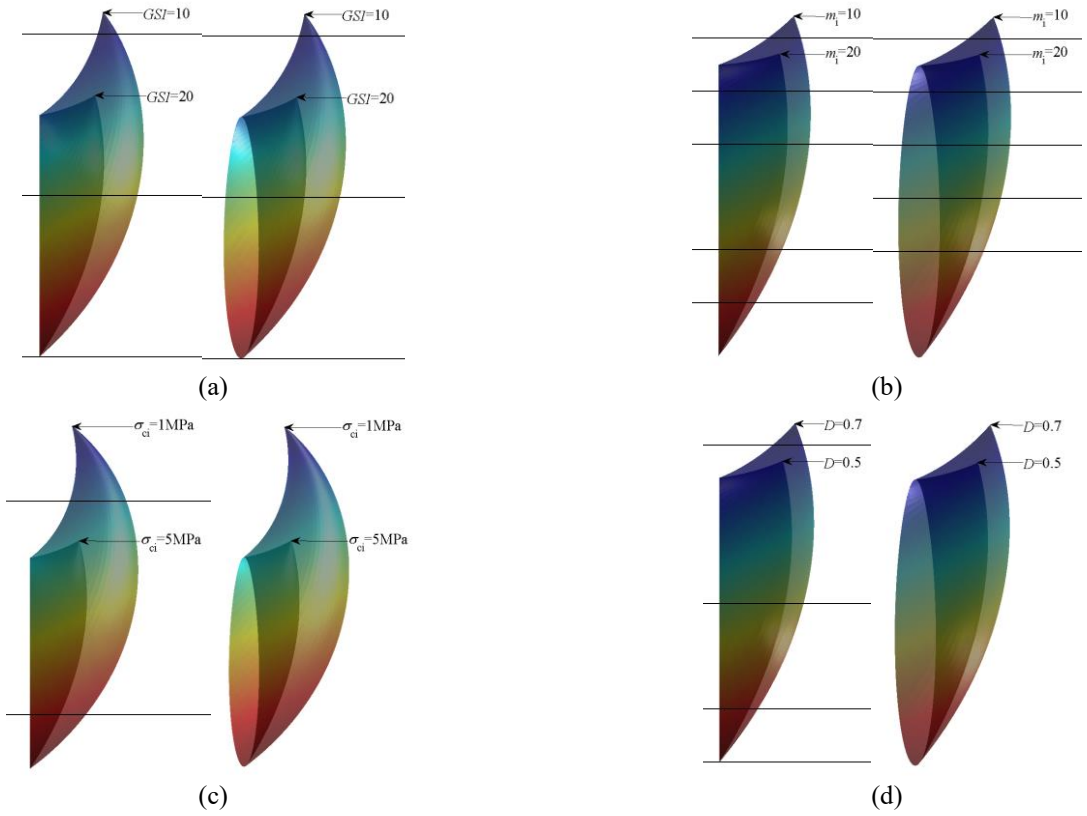

Fig. 4 Influence of Hoek-Brown criterion parameters on the failure range (a) The influence of *GSI*, remaining parameters are γ=25 kN/m^3, d=10 m, m_i=15, σ_{ci}=5 MPa, D=0.7, (b) The influence of m_i, remaining parameters are γ=25 kN/m^3, d=10 m, GSI=20,σ_{ci}=5 MPa, D=0.7,(c) The influence of σ_{ci}, remaining parameters are γ=25 kN/m^3, d=10 m, GSI=20, D=0.7, m_i=15 and (d) The influence of D, remaining parameters are γ=25 kN/m^3, d=10 m, GSI=15, m_i=15, σ_{ci}=5 MPa

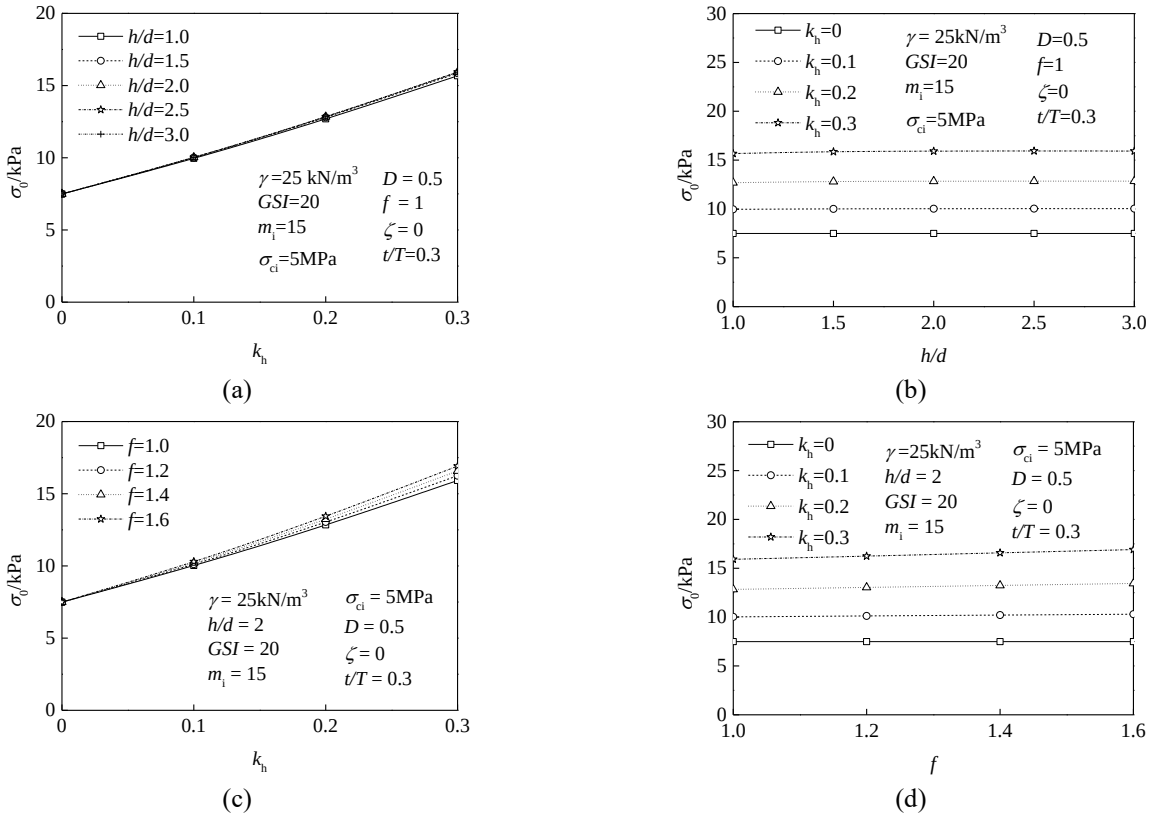

Fig. 5 Effects of parameters on surrounding rock pressure with only horizontal seismic force

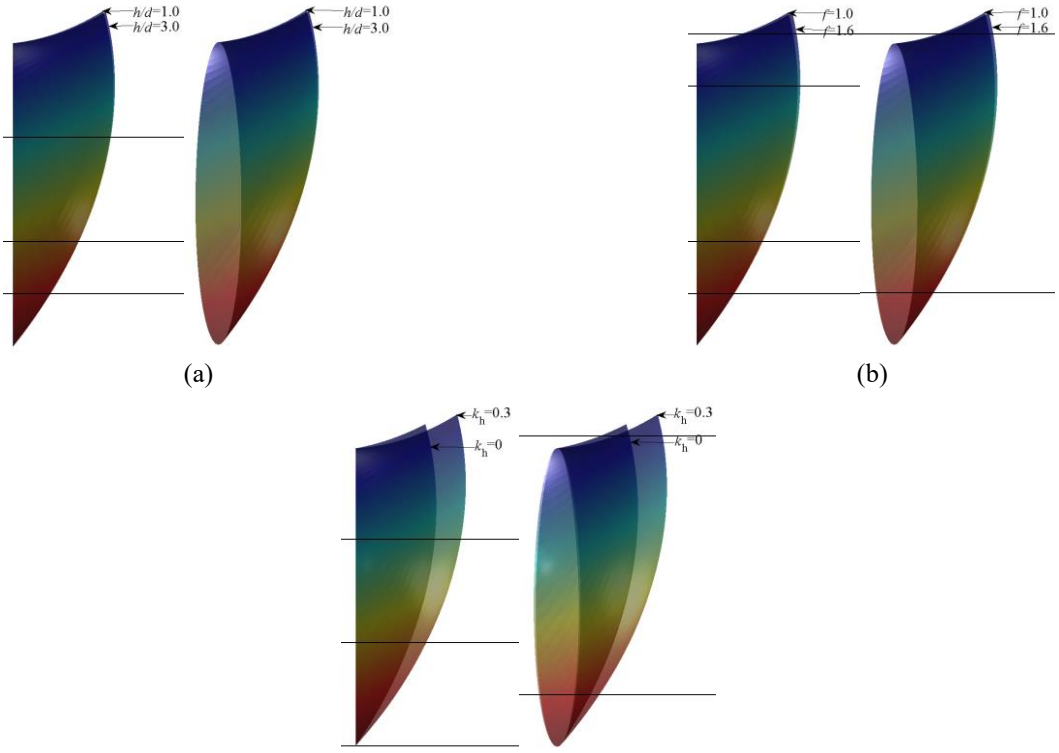

Fig. 6 Effects of parameters on failure range with only horizontal seismic force (a) The influence of h/d, other parameters are γ=25 kN/m^3, GSI=20, m_i=15, σ_{ci}=5 MPa, D=0.7, f=1, k_h=0.2, ζ=0, t/T=0.3, (b) The influence of f, other parameters are γ=25 kN/m^3, h/d=2, GSI=20, m_i=15, σ_{ci}=5 MPa, D=0.7, k_h=0.2, ζ=0, t/T=0.3 and (c) The influence of k_h, other parameters areγ=25kN/m^3, h/d=2, GSI=20, m_i=15, σ_{ci}=5MPa, D=0.7, f=1, ζ=0, t/T=0.3

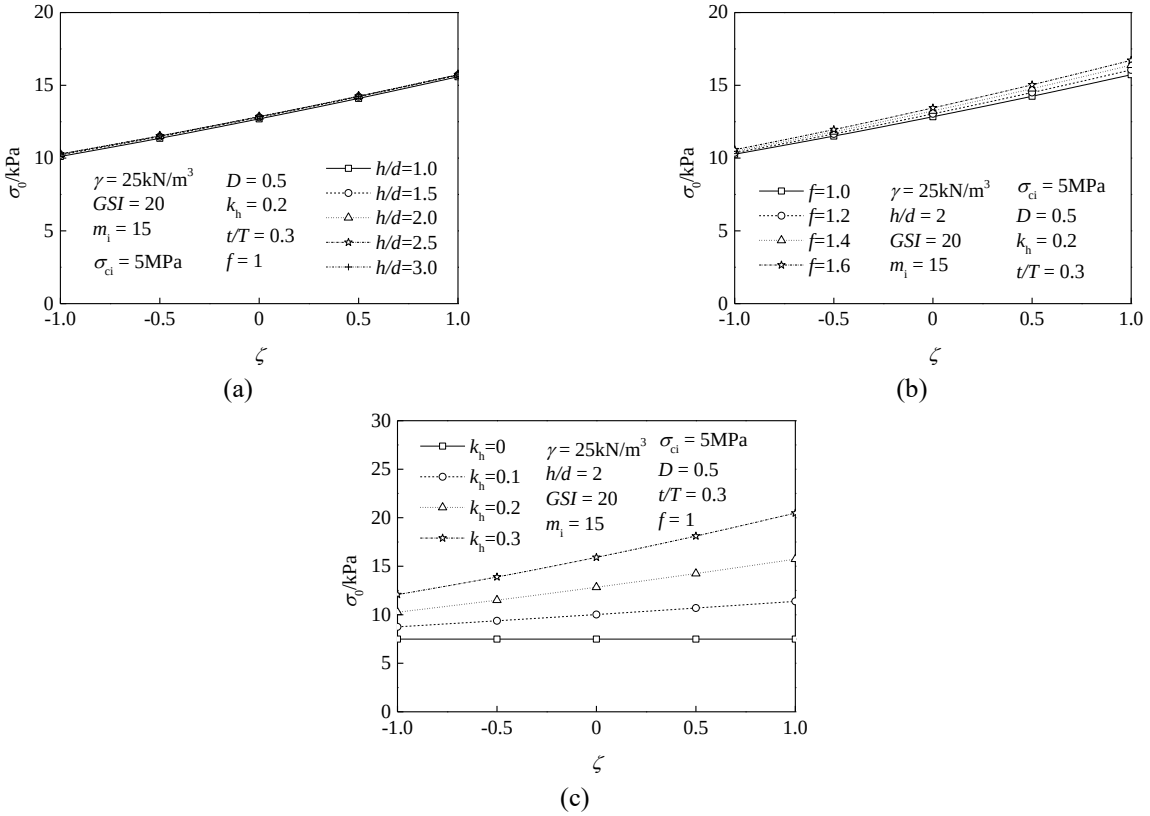

Fig. 7 Effects of parameters on surrounding rock pressure with horizontal and vertical seismic forces

faces are shown in Fig. 5 and Fig. 6, respectively.

As shown in Fig. 5, with the increase of k_h, the surrounding rock pressure σ_0 shows a linear trend of increasing. Therefore, the surrounding rock pressure is being affected dramatically by the horizontal seismic force. With the increase of h/d, the surrounding rock pressure σ_0 does not change obviously, which indicates that h/d has little effect on the surrounding rock pressure when the h/d is small, and the failure surface does not extend to the surface. σ_0 increases linearly with the increase of the magnification coefficient f, but the rising trend is relatively slow. As the magnification factor f increases, the surrounding rock pressure σ_0 increases linearly, but the increasing trend is relatively quiet. This shows that the magnification factor has a specific impact on the surrounding rock pressure. When the assumed sinusoidal wave is not consistent with the actual seismic wave, the amplification factor can be adjusted to make the calculated result close to the real value.

As shown in Fig. 6, the failure range of the tunnel faces increases when k_h increases, which is mainly reflected in the fact that the failure face extends along the direction of excavation, but the apex of the failure block does not change significantly. However, with the increase of h/d and magnification factor f, the failure range of tunnel faces shows subtle changes. It can be seen that h/d and f barely affect the failure range and therefore can be ignored.

4.1.4 Condition with both horizontal and vertical seismic effects

When both horizontal and vertical seismic forces are considered, the effect of vertical acceleration on the surrounding rock pressure and the failure range of tunnel faces is shown in Fig. 7 and Fig. 8, respectively.

As shown in Fig.7, as the vertical acceleration proportional coefficient ζ increases, the surrounding rock pressure σ_0 increases, and significantly the more massive the horizontal acceleration coefficient k_h is, the more pronounced the increasing effect will be. Therefore, the vertical seismic effect has a significant impact in the surrounding rock pressure of the tunnel faces, especially when the horizontal seismic effect has a great effect. However, the buried depth ratio h/d has little influence on σ_0, which can be ignored. The magnification coefficient f has specific impact on σ_0, that is, as f increases, σ_0 increases, but the effect is not remarkable. As shown in Fig 8, with the increase of the proportional coefficient of vertical acceleration ζ, the failure range of the tunnel faces increases. However, this effect is small, which is mainly reflected in the rise of the apex of the failure block and the failure face does not extend significantly along the direction of excavation.

4.2 Permanent displacement

4.2.1 Newmark method

The Newmark method is an effective tool to discuss the seismic stability of the slope. The safety index of the slope is not the minimum safety factor, but the permanent displacement. The Newmark method is introduced into the tunnel. The permanent displacement in the horizontal

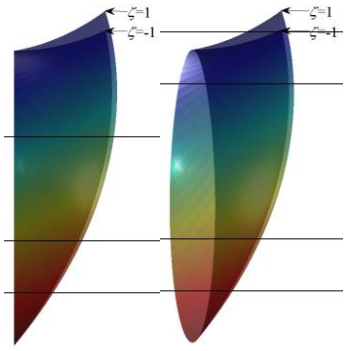

Fig. 8 Effects of proportional coefficient of vertical acceleration ζ on failure range

direction of the tunnel faces can be expressed, after determining yield acceleration a_{cr} and the time-history curves of seismic acceleration $a(t)$ on the sliding block AEB (Yigit 2020, Cattoni *et al*. 2019).

$$s = \iint_t [a(t) - a_{cr}]dtdt \tag{28}$$

where, s refers the horizontal permanent displacement; a_{cr} refers the yield acceleration in the horizontal direction; $a(t)$ refers the time-history curve of seismic acceleration in the horizontal direction, which is equal to $a_h(z,t)$ in Eq. (1) $a(t)=a_h(z,t)$.

4.2.2 Upper bound solution of yield acceleration

To obtain the yield acceleration in the horizontal direction, the horizontal seismic force should be applied to the calculation model shown in Fig. 1. Consequently, the combined effect of horizontal seismic force, gravity and supporting force is applied on the tunnel face, leading to the ultimate failure state. The Newmark method is adopted to apply the horizontal yield acceleration in the 3D calculation model of tunnel faces, and the work rate of the yield acceleration is shown as

$$\begin{aligned} \dot{W_e}' = \frac{a_{cr}}{g}\int_{\theta_2}^{\theta_3} d\theta \int_{-R}^{R} dy \int_{0}^{\sqrt{R^2-y^2}} 2\omega\gamma(r_m+y)^2\cos\theta\, dx + \\ \frac{a_{cr}}{g}\int_{\theta_1}^{\theta_2} d\theta \int_{l}^{R} dy \int_{0}^{\sqrt{R^2-y^2}} 2\omega\gamma(r_m+y)^2\sin\theta\, dx \end{aligned} \tag{29}$$

The yield acceleration can be determined when the external work rate is equal to the internal energy dissipation. Then, by combining Eq. (14), Eq. (16), Eq. (18) and Eq. (29), the analytic solution of the yield acceleration a_{cr} can be obtained.

$$a_{cr} = g\frac{\dot{W}_V - \dot{W}_\gamma - \dot{W}_T}{f_8} \tag{30}$$

where

$$\begin{aligned} f_8 = \int_{\theta_2}^{\theta_3} d\theta \int_{-R}^{R} dy \int_{0}^{\sqrt{R^2-y^2}} 2\omega\gamma(r_m+y)^2\cos\theta\, dx + \\ \int_{\theta_1}^{\theta_2} d\theta \int_{l}^{R} dy \int_{0}^{\sqrt{R^2-y^2}} 2\omega\gamma(r_m+y)^2\sin\theta\, dx \end{aligned} \tag{31}$$

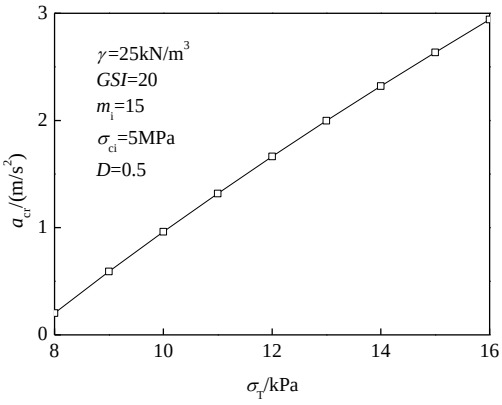

Fig. 9 Relation between yield acceleration and supporting force

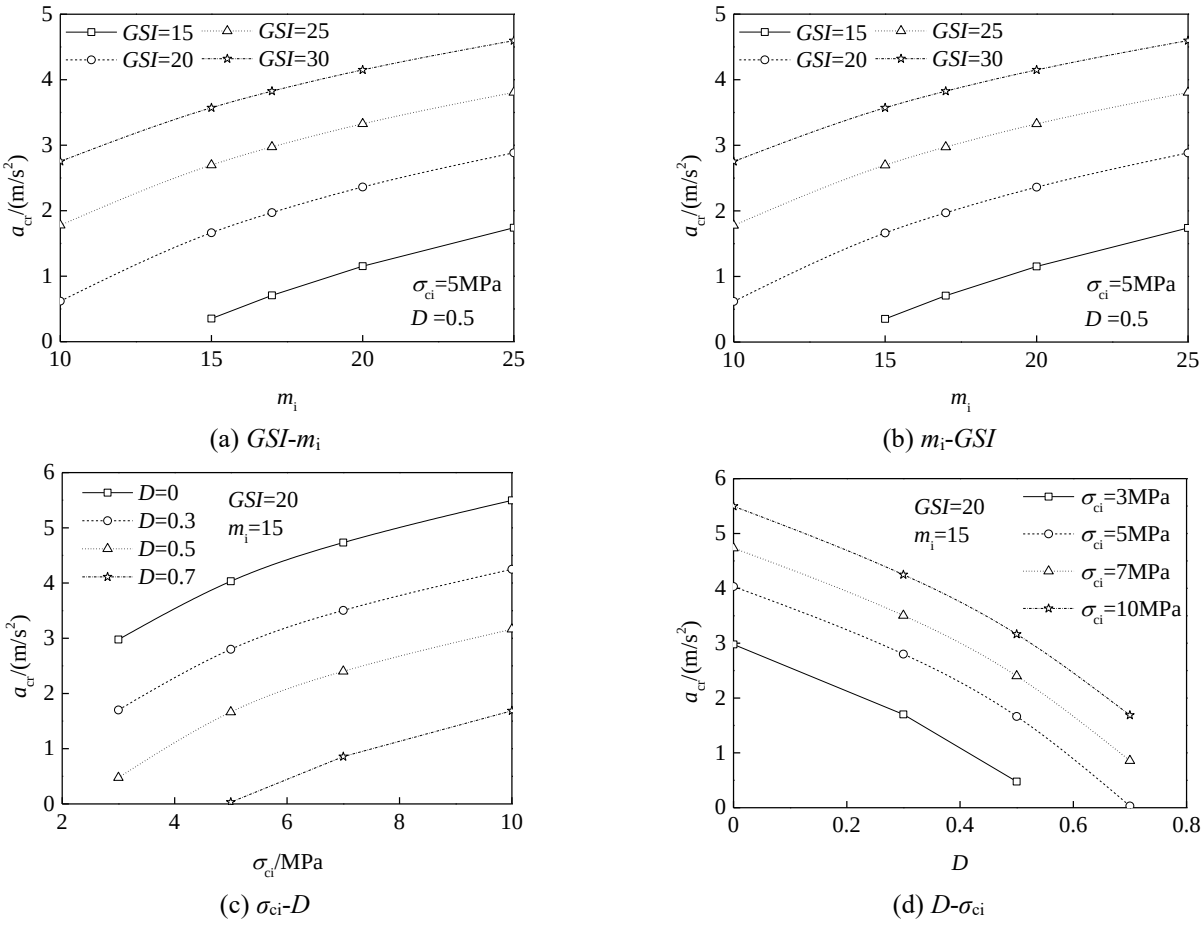

Fig. 10 Effect of rock mass parameters on yield acceleration

Under the constraint of Eq. (27), the minimum value of yield acceleration a_{cr} can be optimized by using Matlab. When the minimum yield acceleration a_{cr} is obtained, the permanent displacement of tunnel face under earthquake action can be solved by substituting this value into Eq. (28) together with the horizontal seismic acceleration $a(t)$, namely, $a_h(z,t)$ in Eq. (1).

4.2.3 Effect of rock mass parameters and supporting force on yield acceleration

According to Eq. (30), yield acceleration a_{cr} is a function of soil mass weight γ, disturbance factor D, rock mass constant m_i, uniaxial compressive strength σ_{ci}, geological strength index GSI and supporting force σ_T, $a_{cr}=f(\gamma, GSI, m_i, \sigma_{ci}, D, \sigma_T)$. When a supporting force σ_T is given to make the tunnel faces in the limit equilibrium state, the applied yield acceleration a_{cr} can be calculated. The effect of supporting force on yield acceleration is shown in Fig. 9. The relevant parameters are as follows: γ=25 kN/m^3, GSI=20, m_i=15, σ_{ci}=5 MPa and D=0.5.

The effect of rock mass parameters on the yield acceleration of the tunnel is shown in Fig 10. The relevant parameters are as follows: γ=25 kN/m^3, σ_T=12 kPa. In Fig. 10, as GSI, m_i and σ_{ci} increase, the yield acceleration a_{cr}

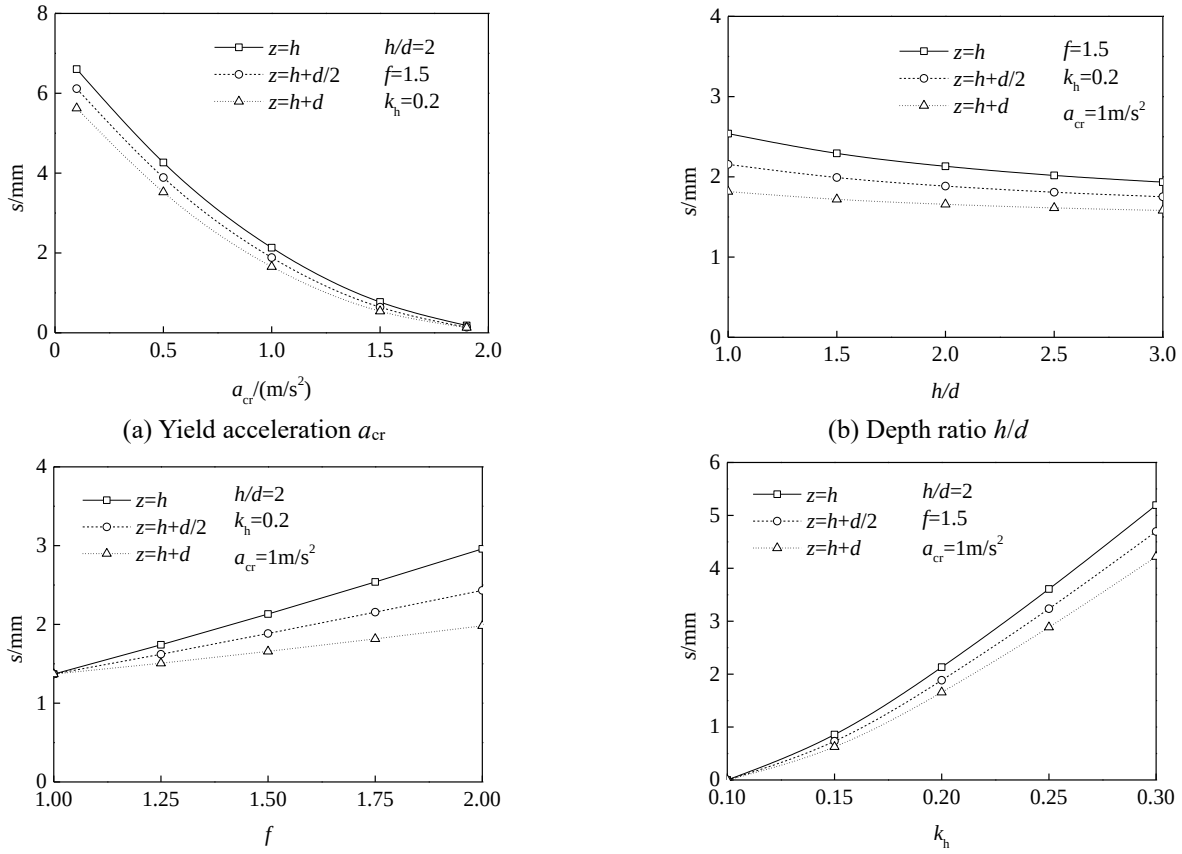

(a) Yield acceleration a_{cr} (b) Depth ratio h/d

(c) Amplification coefficient f (d) Horizontal seismic acceleration coefficient k_h

Fig. 11 Effect of various parameters on the permanent displacement at the top, center and bottom of tunnel faces

Table 2 Permanent displacement at the top, center and bottom of tunnel faces under seismic force

No.	h/d	f	k_h	a_{cr} /(m/s²)	s /mm				
					Bottom (z=h+d)	Center (z=h+d/2)	Relative error(%)	Top (z=h)	Relative error(%)
1	2.0	1.50	0.20	0.1	5.63	6.11	8.5	6.60	17.2
2	2.0	1.50	0.20	0.5	3.52	3.89	10.5	4.27	21.3
3	2.0	1.50	0.20	1.0	1.66	1.88	13.3	2.13	28.3
4	2.0	1.50	0.20	1.5	0.54	0.64	18.5	0.77	42.6
5	2.0	1.50	0.20	1.9	0.13	0.14	7.7	0.18	38.5
6	1.0	1.50	0.20	1.0	1.82	2.16	18.7	2.54	39.6
7	1.5	1.50	0.20	1.0	1.72	1.99	15.7	2.29	33.1
8	2.0	1.50	0.20	1.0	1.66	1.88	13.3	2.13	28.3
9	2.5	1.50	0.20	1.0	1.61	1.81	12.4	2.02	25.5
10	3.0	1.50	0.20	1.0	1.58	1.75	10.8	1.93	22.2
11	2.0	1.00	0.20	1.0	1.37	1.37	0	1.37	0
12	2.0	1.25	0.20	1.0	1.51	1.62	7.3	1.74	15.2
13	2.0	1.50	0.20	1.0	1.66	1.88	13.3	2.13	28.3
14	2.0	1.75	0.20	1.0	1.82	2.16	18.7	2.54	39.6
15	2.0	2.00	0.20	1.0	1.98	2.43	22.7	2.96	49.5
16	2.0	1.50	0.10	1.0	0	0	0	0	0
17	2.0	1.50	0.15	1.0	0.63	0.73	15.9	0.86	36.5
18	2.0	1.50	0.20	1.0	1.66	1.88	13.3	2.13	28.3
19	2.0	1.50	0.25	1.0	2.89	3.24	12.1	3.61	24.9
20	2.0	1.50	0.30	1.0	4.22	4.70	11.4	5.19	23.0

increases nonlinearly, and the increasing trend gradually slows down. While as the disturbance factor D increases, the yield acceleration a_{cr} decreases nonlinearly, and the decreasing trend becomes steeper. Therefore, the parameters of Hoek-Brown criterion have a significant effect on the yield acceleration. The assumed yield acceleration and supporting force make the tunnel faces structure in the ultimate failure state. Therefore, when the supporting force is constant, the worse the rock mass strength characteristics characterized by Hoek-Brown criterion parameters are, the smaller the yield acceleration can make the tunnel faces structure in the ultimate failure state. Conversely, the yield acceleration depends on the strength characteristics of the rock mass, that is, the parameters of Hoek-Brown criterion of the rock mass.

4.2.4 Permanent displacement of a particle on the tunnel faces

As shown in Eq. (1) and Eq. (28) that the permanent displacement s is a function of yield acceleration a_{cr}, buried depth ratio h/d, amplification factor f, horizontal seismic acceleration coefficient k_h and particle position z, $s=f(a_{cr}, h/d, f, k_h, z)$. The effect of these parameters on the permanent displacement of the three positions of the top ($z=h$), center ($z=h+d/2$) and bottom ($z=H=h+d$) of the tunnel faces are shown in Fig. 11 and the relevant data is shown in Table 2.

As shown in Fig. 11, with the increase of yield acceleration a_{cr} or depth ratio h/d, the permanent displacement s decreases nonlinearly, and the decreasing trend gradually slows down. The difference is that, compared with the depth ratio h/d, the yield acceleration a_{cr} has a more substantial impact on the permanent displacement, indicating that the yield acceleration a_{cr} has a significant effect on the permanent displacement s. In contrast, the depth ratio h/d has a relatively small effect on the permanent displacement removal s. According to Eq. (1) and Eq. (33), under a specific seismic acceleration $a(t)$, the yield acceleration a_{cr} increases, this means that the critical acceleration value capable of generating displacement increases, so the permanent displacement decreases. Similarly, under the condition of certain yield acceleration a_{cr}, when h/d increases, the amplitude of seismic acceleration $a(t)$ decreases, so the permanent displacement decreases.

Table 2 shows the permanent displacement at the top, center, and bottom of tunnel faces under earthquake action. It can be seen from Table 2 that the permanent displacement at the bottom of the tunnel faces is the smallest, the permanent displacement at the center is the middle, and the permanent displacement at the top is the largest. Take the parameters of NO.1 to illustrate, the permanent displacement of the bottom of the tunnel faces is 5.63 mm, the permanent displacement of the center is 6.11 mm, and the permanent displacement of the top is 6.60 mm. Take the permanent displacement at the bottom as a reference, the difference between the permanent displacement at the center and the top is 0.48 mm and 0.97 mm, and the relative error is 8.5% and 17.2, respectively. The larger the distance of the particle from the earth surface, the smaller the amplitude of seismic acceleration, and the smaller the permanent displacement when the yield acceleration is constant. It shows that the distance from the surface has a great effect on the permanent displacement.

6. Conclusions

• The time-domain waveform of surrounding rock pressure of soft rock tunnel under seismic force was obtained by the quasi-static method and the pseudo-dynamic method, respectively. The results showed that the maximum solution and the minimum solution of the surrounding rock pressure calculated by the pseudo-dynamic method were around 0.3T and 0.8T, respectively. And the maximum solution was equal to the solution of the surrounding rock pressure calculated by the quasi-static method.

• The situations without seismic force and with the horizontal and vertical seismic forces are considered, respectively. The effects of the parameters of Hoek-Brown strength criterion and pseudo-dynamic approach on surrounding rock pressure and failure range of the tunnel faces were investigated. The results showed that the surrounding rock pressure decreases with the increase of GSI, m_i and σ_{ci}, increases as the horizontal acceleration coefficient and the vertical acceleration coefficient increased, and had not changed with the depth of the tunnel. The failure range decreases with the rise of GSI, m_i and σ_{ci}, increases with the increase of disturbance factor D, horizontal acceleration coefficient, and vertical acceleration proportional coefficient. At the same time, it is independent of the change of burial depth and amplification factor.

• According to the stability calculation model of tunnel faces under seismic force, the minimum yield acceleration under limit state were calculated. The effects of rock mass parameters and supporting force on yield acceleration was analyzed. The results suggested that the yield acceleration increases when the rock mass constant and uniaxial compressive strength increases, and it decreases as the disturbance factor increases.

• The permanent displacement of top, center and bottom of tunnel faces was calculated by the Newmark method, and the influence of relevant parameters on the permanent displacement of the three positions of tunnel faces was discussed. As the results showed, the permanent displacement decreases with yield acceleration, buried depth, horizontal acceleration coefficient and amplification coefficient. The difference of the permanent displacement between center and bottom, the top, and the bottom of the tunnel faces was 0.48mm and 0.97mm, respectively. The relative errors were 8.5% and 17.2, respectively.

Acknowledgments

The preparation of this work received financial support from the National Natural Science Foundation of China (52004088, 51804113 and 52074116) and the Science Foundation of Hunan University of Science and Technology (E52076).

References

Abate, G. and Massimino, M.R. (2017), "Parametric analysis of the seismic response of coupled tunnel-soil-aboveground building systems by numerical modeling", *B. Earthq. Eng.*, **15**(1), 443-467. https://doi.org/10.1007/s10518-016-9975-7.

Basha, B.M. and Babu G.L.S. (2010), "Reliability assessment of internal stability of reinforced soil structures: A pseudo-dynamic approach", *Soil Dyn. Earthq. Eng.*, **30**(5), 336-353. https://doi.org/10.1016/j.soildyn.2009.12.007.

Cattoni, E., Salciarini, D. and Tamagnini, C. (2019), "A generalized Newmark method for the assessment of permanent displacements of flexible retaining structures under seismic loading conditions", *Soil Dyn. Earthq. Eng.*, **117**, 221-233. https://doi.org 10.1016/j.soildyn.2018.11.023.

Chanda, N., Ghosh, S. and Pal, M. (2019), "Seismic stability of slope using modified pseudo-dynamic method", *Int. J. Geotech. Eng.*, **13**(6), 548-559. https://doi.org/10.1080/19386362.2017.1372056.

Eskandarinejad A. and Shafiee A.H. (2011), "Pseudo-dynamic analysis of seismic stability of reinforced slopes considering non-associated flow rule", *J. Central South Univ.*, **18**(6), 2091-2099. https://doi.org/10.1007/s11771-011-0948-3.

Fraldi, M., Guarracino, F. (2012), "Limit analysis of progressive tunnel failure of tunnels in Hoek-Brown rock masses", *Int. J. Rock Mech. Min. Sci.*, **50**, 170-173. https://doi.org/10.1016/j.ijrmms.2011.12.009.

Hoek, E., Carranza-Torres, C. and Corkum, B. (2002), "Hoek-Brown failure criterion—2002 edition", *Proceedings of the North American Rock Mechanics Society Meeting*, Toronto, Canada, January.

Huang, F., Feng, Y., Zhang, Z.Q., Yang, X.L. and Ling, T.H. (2019), "Upper bound solution of the safety factor for a shield tunnel face subjected to the Hoek-Brown failure criterion", *Int. J. Civ. Eng.*, **17**(12), 1941-1950. https://doi.org/10.1007/s40999-019-00416-3.

Ibrahim, E., Soubra, A.H., Mollon, G., Raphael, W., Dias, D. and Reda, A. (2015), "Three-dimensional face stability analysis of pressurized tunnels driven in a multilayered purely frictional medium", *Tunn. Undergr. Sp. Tech.*, **49**(1), 18-34. https://doi.org/10.1016/j.tust.2015.04.001.

Jishnu, R.B., Ramanathan, A., Ahmed, S., Chayan, P. and Ghosh, S. (2016), "Performance of primary tunnel support systems under seismic loads in weak rock masses", *Proceedings oftThe Conference on Recent Advances in Rock Engineering* (*RARE* 2016), Bengaluru, India, November.

Khezri, N., Mohamad, H., HajiHassani, M. and Fatahi, B. (2015), "The stability of shallow circular tunnels in soil considering variations in cohesion with depth", *Tunn. Undergr. Sp. Tech.*, **49**(7), 230-240. https://doi.org/10.1016/j.tust.2015.04.014.

Kumar, J. and Rahaman, O. (2020), "Lower bound limit analysis of unsupported vertical circular excavations in rocks using Hoek-Brown failure criterion", *Int. J. Numer. Anal. Met.*, **44**(10), 1093-1106. https://doi.org/10.1002/nag.3051.

Michalowski R.L. and Nadukuru S.S. (2013), "Three-dimensional limit analysis of slopes with pore pressure", *J. Geotech. Geoenviron. Eng.*, **139**(9), 1604-1610. https://doi.org/10.1061/(ASCE)GT.1943-5606.0000867.

Mollon, G., Dias, D. and Soubra A.H. (2010), "Face stability analysis of circular tunnels driven by a pressurized shield", *J. Geotech. Geoenviron. Eng.*, **136**(1), 215-229. https://doi.org/10.1061/(ASCE)GT.1943-5606.0000194.

Munwar, B.B. and Sivakumar, B.G.L. (2009). "Computation of sliding displacements of bridge abutments by pseudo-dynamic method", *Soil Dyn. Earthq. Eng.*, **29**(1), 103-120. https://doi.org/10.1016/j.soildyn.2008.01.006.

Nadukuru, S.S. and Michalowski, R.L. (2013), "Three-dimensional displacement analysis of slopes subjected to seismic loads", *Can. Geotech. J.*, **50**(6), 650-661. https://doi.org/10.1139/cgj-2012-0223.

Pakbaz, M.C. and Yareevand, A. (2005), "2-D analysis of circular tunnel against earthquake loading", *Tunn. Undergr. Sp. Tech.*, **20**(5), 411-417. https://doi.org/10.1016/j.tust.2005.01.006.

Pan, Q.J. and Dias, D. (2018), "Three-dimensional static and seismic stability analysis of a tunnel face driven in weak rock ,asses", *Int. J. Geomech.*, **18**(6), 04018055. https://doi.org/10.1061/(ASCE)GM.1943-5622.0001174.

Saada, Z., Maghous, S. and Garnier, D. (2013), "Pseudo-static analysis of tunnel face stability using the generalized Hoek-Brown strength criterion", *Int. J. Numer. Anal. Met.*, **37**(18), 3194-3212. https://doi.org/10.1002/nag.2185.

Senent, S., Mollon, G. and Jimenez, R. (2013), "Tunnel face stability in heavily fractured rock masses that follow the Hoek-Brown failure criterion", *Int. J. Rock Mech. Min. Sci.*, **60**(1), 440-451. https://doi.org/10.1016/j.ijrmms.2013.01.004.

Soubra, A.H. (2002), "Kinematical approach to the face stability analysis of shallow circular tunnels", *Proceedings of the 8th International Symposium on Plasticity*, British Columbia, Canada, July.

Subrin, D. and Wong, H. (2002), "Tunnel face stability in frictional material: A new 3D failure mechanism", *Comptes Rendus Mecanique*, **330**(7), 513-519. https://doi.org/10.1016/S1631-0721(02)01491-2.

Wang, K.H, Ma, S.J. and Wu, W.B (2011). "Pseudo-dynamic analysis of overturning stability of retaining wall", *J. Central South Univ.*, **18**(6), 2085-2090. https://doi.org/10.1007/s11771-011-0947-4.

Yigit, A. (2020), "Prediction of amount of earthquake-induced slope displacement by using Newmark method", *Eng. Geol.*, **264**, 105385. https://doi.org/10.1016/j.enggeo.2019.105385.

Zhang, B., Ma, Z.Y. and Wang, X. (2020), "Reliability analysis of anti-seismic stability of 3D pressurized tunnel faces by response surfaces method", *Geomech. Eng.*, **20**(1), 43-54. https://doi.org/10.12989/gae.2020.20.1.043.

Zhang, D.B. and Zhang, B. (2020), "Stability analysis of the pressurized 3D tunnel face in anisotropic and nonhomogeneous soils", *Int. J. Geomech.*, **20**(4), 04020018. https://doi.org10.1061/(ASCE)GM.1943-5622.0001635.

Zhang, D.B., Jiang, Y. and Yang, X.L. (2019), "Estimation of 3D active earth pressure under nonlinear strength condition", *Geomech. Eng.*, **17**(6), 515-525. https://doi.org/10.12989/gae.2019.17.6.515.

Zhang, J.H., Wang, W.J., Zhang, D.B., Zhang, B. and Meng, F. (2018), "Safe range of retaining pressure for three-dimensional face of pressurized tunnels based on limit analysis and reliability method", *KSCE J. Civ. Eng.*, **22**(11), 4645-4656. https://doi.org/10.1007/s12205-017-0619-5.

Zhang, J.H. and Zhang, B. (2019), "Reliability analysis for seismic stability of tunnel faces in soft rock masses based on a 3D stochastic collapse model", *J. Central South Univ.*, **26**(7), 1706-1718. https://doi.org/10.1007/s11771-019-4127-2.

Zhang, J.H., Zhang, L.Y., Wang, W.J., Zhang, D.B. and Zhang, B. (2020), "Probabilistic analysis of three-dimensional tunnel face stability in soft rock masses using Hoek-Brown failure criterion", *Int. J. Numer. Anal. Met.*, **44**(11), 1601-1616. https://doi.org/10.1002/nag.3085.

CC